

This is the accepted version of:

[S I Imbriglio et al 2019 Surf. Topogr.: Metrol. Prop. 7 045002 DOI: 10.1088/2051-672X/ab3efc](#)

## **Failure dynamics of spherical and irregular shaped Ti splats deposited on sapphire by cold spray**

**S. I. Imbriglio<sup>1</sup>, V.N.V. Munagala<sup>1</sup>, T. Schmitt<sup>2</sup>, R. Gauvin<sup>1</sup>, J. E. Klemberg-Sapieha<sup>2</sup>, R. R. Chromik<sup>1,\*</sup>**

<sup>1</sup> Department of Mining and Materials Engineering, McGill University, 3610 University Street, Montreal, QC, H3A 0C5, Canada

<sup>2</sup> Department of Engineering Physics, Polytechnique Montreal, P.O. Box 6079, Station Centre-ville, Montreal, Quebec, H3C 3A7, Canada

\* Corresponding author. Telephone: +1(514) 398-5686; Fax: +1 (514) 398-4492

Email address: [richard.chromik@mcgill.ca](mailto:richard.chromik@mcgill.ca)

This is the accepted version of:

[S I Imbriglio et al 2019 Surf. Topogr.: Metrol. Prop. 7 045002 DOI: 10.1088/2051-672X/ab3efc](#)

Declarations of interest: none

## Abstract

Single splats of commercially pure (CP) Ti are deposited onto sapphire by cold spray under two spray conditions to achieve different in-flight powder velocities. The powders used have two morphologies: spherical powder (SP), manufactured by plasma gas atomization and irregular powder (IP), manufactured by the Armstrong process, with a coral-like morphology. The adhesion strength of the single splats is measured by splat adhesion testing. By use of a specialized *in situ* scratch tester, interface failure during splat adhesion testing is observed through the sapphire substrate. Particle velocity does not significantly influence the adhesion strength and failure mechanism of SP splats. After deposition, the SP splat has an interface pore in its center which acts as an initiation site for crack propagation during splat adhesion testing. After failure, a well bonded portion of Ti remains on the substrate in the shape of a ring. IP splats deposited at low velocity show similar, well adhering, rings on the surface in localized locations scattered throughout the interface. An increase in velocity for IP splats led to an increase in adhesion strength and a nearly continuous well adhering interface. The behaviour of IP splats is understood by electron channelling contrast images of cross-sections where low velocities resulted in little change in microstructure while high velocities led to a highly deformed microstructure at the interface.

**Keywords** cold spray; irregular powder; spherical powder; sapphire substrate; titanium powder; metal/ceramic interface

## 1. Introduction

During cold spray deposition, micro-particle impact onto a substrate allows for coating buildup. The micro-particles adhering to the substrate are referred to as “splats”. Coating properties are directly affected by cohesion between splats and adhesion of splats to the substrate. Testing of adhesion and cohesion of coatings is typically done by bulk mechanical testing in tension [1-5]. When investigating new coating/substrate combinations, information pertaining to the ideal deposition conditions and adhesion strength at the interface is sought. Bulk mechanical testing in tensions has several drawbacks for this application including the use of a lot of powder, machining of specific substrate geometries and failure away from the coating/substrate interface [6]. The latter drawbacks are of particular concern when investigating adhesion between metal coatings and ceramic substrates. Interest in metal/ceramic interfaces deposited by cold spray stems from their advantageous properties in metal matrix composite coatings [7] and potential applications in ceramic metallization [8-11]. With little known regarding the required spray conditions to deposit a dense and well adhering coating, a lot of wasted powder is expected if using a tensile test. Specific substrate geometries may also be difficult or expensive to manufacture out of ceramic. Failure of the ceramic in tension rather than at the interface may prevent a proper investigation of interface failure. For a more direct study of interface characteristics, Chromik et al. introduced a splat adhesion test which is an experimental technique adapted from the ball bond shear test, typically used to investigate adhesion of solder balls in microelectronics, to quantitatively study the adhesion of single cold sprayed splats [6].

The splat adhesion test has been successful in characterizing adhesion in metal/ceramic interfaces (i.e. Ti/Al<sub>2</sub>O<sub>3</sub> and Ti/SiC interfaces) [12, 13]. Post-test characterization using light optical microscopy (LOM) and scanning electron microscopy (SEM) images of failed interfaces provides information regarding factors contributing to adhesion. Substrate morphology and substrate composition have been found to influence the appearance of failed interfaces [12, 13]. Splat adhesion testing of Ti splats deposited on polycrystalline Al<sub>2</sub>O<sub>3</sub> revealed differences in bonding mechanism with different substrate morphologies [12]. Ti formed a bond at the periphery of the splat when deposited on polished polycrystalline substrates. On rough substrates the Ti penetrated into the asperities to form a mechanical bond [12]. The bond formed along the periphery of the splat on polished substrates covered a larger contact area than the localized mechanical bonding

on rough substrate rendering an overall higher adhesion strength. It was assumed that the bond formed in the periphery of the splats on polished substrates is from chemico-physical interactions between the metal and ceramic during the formation of adiabatic shear instabilities (ASI) and jetting at impact because no mechanical interlocking could occur in these interfaces [12]. The formation of a bond in the periphery of the splat and a gap at the center is characteristic of cold sprayed SP and has been observed in many metal/metal [14-17] and metal/ceramic [10, 17] interfaces. A peripheral bond reflective of that found in Ti/Al<sub>2</sub>O<sub>3</sub> interfaces was also observed in post-test characterization of failed interface between Ti splats deposited on a relatively smooth as-received SiC substrate but only in localized regions of the periphery resulting in a weak adhesion strength [12].

Given the high adhesion strength between Ti splats and polished Al<sub>2</sub>O<sub>3</sub> substrate or atomically smooth sapphire, these interfaces remain of interest for potential industrial application [12, 18]. Yet, the cost of spherical Ti powder is often prohibitively high. The Armstrong process is a novel technique for manufacturing irregular shaped Ti and Ti alloy powders with a coral-like morphology at a fraction of the cost [19]. Depositing irregular Ti powder onto Ti substrates results in dense coatings at lower velocities than SP [19]. Similar results are observed when depositing Ti6Al4V IP onto Ti6Al4V substrates [20]. The superior density of coatings deposited using Armstrong powder is attributed to its shape and microstructure which allows for better deformability and higher velocities for a given spray condition as compared to SP [19, 20]. However, their performance in metal/ceramic interface remains unknown. The irregular shape of the powder was previously found to be advantageous in metal/metal interfaces as they promote compaction and mechanical bonding [19-21]. When deposited at low velocities, metallurgical bonding was not achieved as revealed by weak microhardness measurements with debonding between the splats [19]. Jetting and ASI have been observed for these powders but they appear localized as compared to SP [21]. Given the importance of jetting and ASI in forming a strong bond on a smooth ceramic substrate, it is unclear if the irregular, coral-like, morphology of the powder will be advantageous or detrimental to the formation of a strong bond.

In this work, single splats of spherical and irregular Ti powder are deposited onto optical sapphire windows. These powders are compared in terms of their adhesion strength as measured by the

splat adhesion test for two different spray conditions. Rather than only relying on post-test characterization to understand the bonding mechanism, the transparent nature of the optical sapphire window allows for the use of an *in situ* splat adhesion test where failure dynamics are characterized as the tip interacts with the splat. Adhesion strength measurements and bonding mechanisms are explained through the failure mechanism, post-test characterization and cross-sectional imaging.

## 2. Experimental procedure

Single splats were deposited using spherical and irregular shaped, commercially pure, Ti powder particles by cold spray (PCS-800, Plasma Giken, Saitama, Japan) onto sapphire (Meller optics, Rhode Island, USA) substrates. To deposit single splats by cold spray, nitrogen, with an initial gas pressure of 4 MPa and pre-heat temperature of 400 °C and 800 °C, is used as the carrier gas for both powder morphologies. Hereafter, samples are identified by the gas pre-heat temperature as pressure is maintained constant in both spray conditions. The in-flight velocity of the powder is measured by a time-of-flight particle diagnosis system (Coldspraymeter, Tecnar Automation, Canada). To ensure the deposition of scattered single splats, the gun traverse speed is 1 m/s with the lowest possible feed rate.

The sapphire substrates have a diameter of 11 mm and thickness of 5 mm. The surface of the sapphire substrate has a C-Plane (0001) crystallographic orientation. The SP, with an average particle size of 29 μm, is manufactured by plasma gas atomization and has been characterized elsewhere [12]. The irregular shaped Ti powder (Cristal metals, USA) is manufactured by the Armstrong process and has a coral-like morphology with an average size of 66 μm (figure 1). The IP's coral-like morphology, in the cross-section, shows large, irregularly shaped pores with equiaxed grains. Some grains show minor evidence of deformation (figure 2). The deformation may be due to ball milling, a post processing technique used to target specific tap densities and particles size distributions [22]. There is also a large variation in grain size heterogeneously distributed throughout the microstructure of individual powder particles. Grains range from hundreds of nanometers to few microns (figure 2).

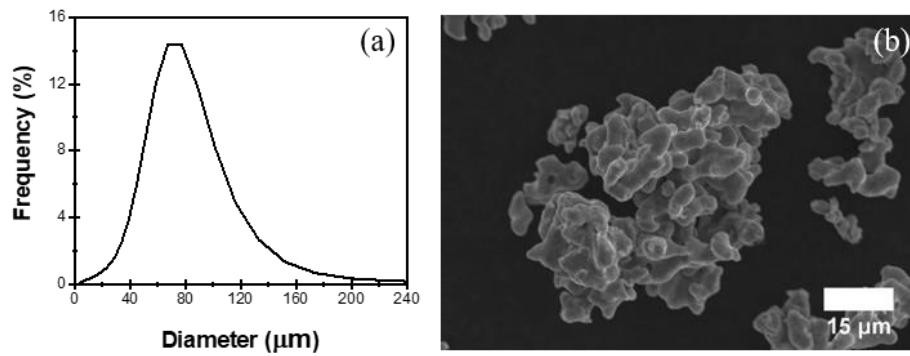


**Figure 1.** The (a) powder size distribution and (b) morphology of the IP manufactured by the Armstrong process.

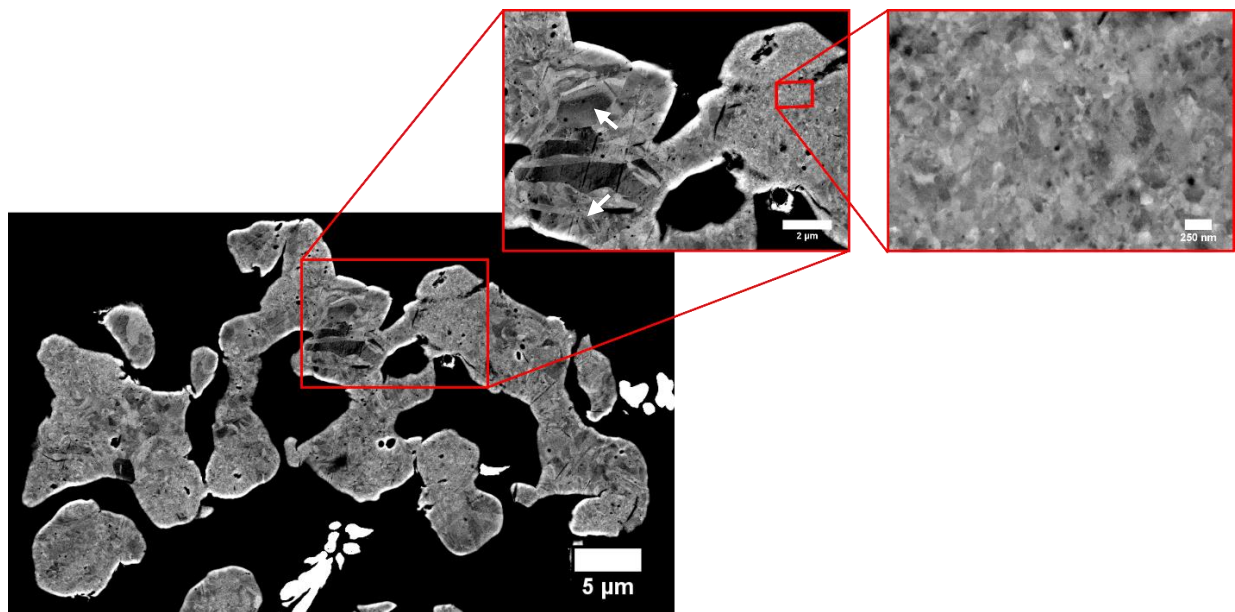


**Figure 2.** The microstructure of the IP manufactured by the Armstrong process. Arrows have been used to emphasize grains showing minor evidence of deformation.

Coating buildup is dependent on initial interactions occurring at the splat level. As such, the study of adhesion of single splats is required to better understand the deposition process. Yet, to date, there is no standardized testing methodology for testing the adhesion of single micron-sized particles. Chromik et al. proposed a technique for testing single splats which is based on the commonly used ball bond shear test for solder balls [6]. This technique has been referred to in

previous works as a splat adhesion test [12, 13, 15]. While failure under the applied load is not completely in tension (mode I) or in shear (mode II) as traditional adhesion testing techniques, results from this technique, accompanied by extensive post-test characterization, are useful to characterize the deposition process and bonding mechanism. The splat adhesion testing methodology, used here, is the same as found in Chromik et al. [6]. A tip with a semi-circular cross-section of 100  $\mu\text{m}$  in diameter is used to scratch the single splats. The sliding speed is fixed to 150  $\mu\text{m}/\text{min}$  and the normal force is set to 100 or 200 mN for all tests. The higher normal force is only used for IP splats deposited at 800°C as the tip consistently traveled over the splat with a lower normal force. The scratch length varies based on the available space between the splats and size of the splats tested. As the tip removes the splat, the tangential force on the tip is recorded. The tangential force records a baseline ( $F_{T \text{ Baseline}}$ ) due to friction between the tip and the substrate and a peak force ( $F_{T \text{ Peak}}$ ) when the tip removes the splat. From these results a splat adhesion strength is calculated using eq. 1 [6].

$$\text{Splat Adhesion Strength [MPa]} = \frac{F_{T \text{ Peak [mN]}} - F_{T \text{ Baseline [mN]}}}{\text{Projected Area } [\mu\text{m}^2]} * 1000 \quad (1)$$

For SP, the projected area is measured using the diameter of the impacted splat prior to each test. The projected area of irregular shaped splats is measured by image processing of LOM images in ImageJ. The tangential force plots with respect to positions and projected areas are also used to calculate splat adhesion energy by eq. 2 [6]. Splat adhesion energy is used to distinguish between a more brittle or more ductile failure of the splats [6].

$$\text{Splat Adhesion Energy [KJ m}^{-2}\text{]} = \frac{\int_{\text{Contact}}^{\text{Failure}} [F_T(x) - F_{T \text{ Baseline}}] dx \text{ [mN} \cdot \mu\text{m]}}{\text{Projected Area } [\mu\text{m}^2]} * 1000 \quad (2)$$

Splat adhesion testing is completed on both an *in situ* and *ex situ* platform. *In situ* splat adhesion testing is performed on a modified Micro-Scratch Tester (CSM Instruments, Inc, Graz, Austria) with an optical setup allowing for observation of the contact area through the transparent substrate. Between 5 and 10 splats are tested for each spray condition using the *in situ* setup. Experiments completed on the *in situ* setup are used to understand fractography of a splat during splat adhesion testing. To ensure consistency between the data presented here and other work [6, 12, 15], the

Micro-Combi Tester (Anton Paar, Graz, Austria) was also used to test at least 15 splats. Results were compared for splats tested with the two equipment. Splat adhesion strength measurements taken with the *in situ* system were higher than the average splat adhesion strength with the *ex situ* system. This difference was due to differences in the measurement of splat area from above (*ex situ*) versus beneath (*in situ*) the splat. When this difference was taken into account, the measurements from the two systems were consistent with one another. Nevertheless, because all previous reports using this technique are on *ex situ* testing, reported splat adhesion strength measurements and tangential force versus position plots are shown for experiments completed on the Micro-Combi Tester. Alongside these results, observations of splat failure are presented from *in situ* testing.

Splats are imaged prior and post splat adhesion testing by a variable-pressure SEM (VP-SEM, SU-3500, Hitachi, Tokyo, Japan). Charging caused by the ceramic substrate is reduced by maintaining a pressure of 40 Pa and an accelerating voltage of 5 kV in the VP-SEM [23]. Powder cross-sections are imaged by a high-pressure SEM (SEM, SU-8230, Hitachi, Tokyo, Japan). Also, to better understand IP splat adhesion test results, focus ion beam milling (FIB) is used to cross-section single IP splats deposited on sapphire. FIB and imaging for these particles is completed on a FEI Helios NanoLab 660 electron microscope located at the Facility for Electron Microscopy Research at McGill University.

### 3. Results

#### 3.1. Cold sprayed splats

Consistent with previous literature [19, 20], IP has a higher in-flight velocity than SP for a specific spray condition (Table 1). Due to their shape, IP experiences more drag than SP resulting in higher in-flight velocities [20]. In this case, the velocity difference is more pronounced using a gas preheat temperature of 400°C.

**Table 1** Velocity of IP and SP for each spray condition

Spray Conditions	Average Particle Velocity (m/s)	
	SP	IP
4.0 MPa, 400°C	491 ± 127	581 ± 80
4.0 MPa, 800°C	692 ± 133	710 ± 91

The morphology of impacted splats is shown in figure 3. SP splats show evidence of jetting along the periphery of the powder (figure 3 (a-b)). Jetting is more pronounced for SP splats deposited at 800°C as compared to SP deposited at 400°C. IP splats, deposited at 400°C, show localized evidence of jetting around the splat (figure 3 (c)) while IP splats deposited at 800°C, show more generalized jetting around the splat (figure 3 (d)).

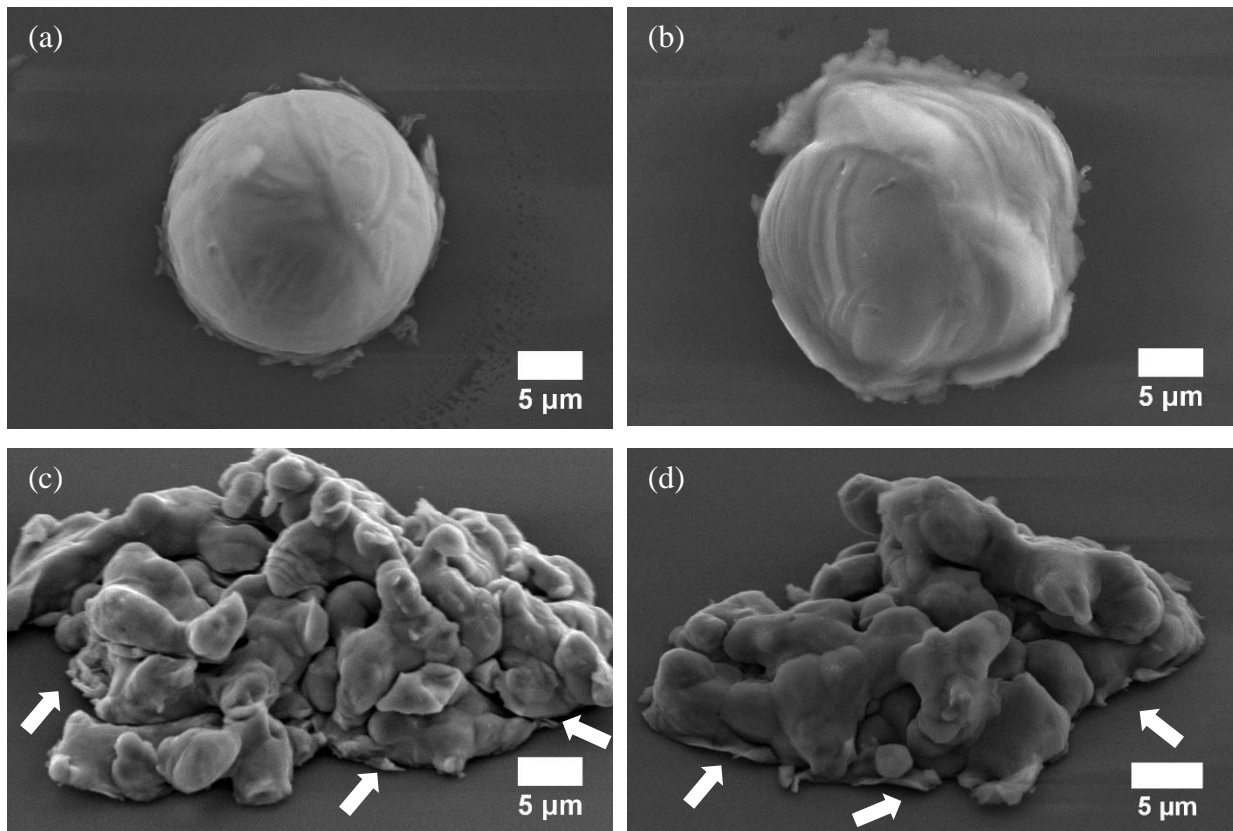


**Figure 3.** Morphology of SP deposited with a gas preheat temperature of (a) 400°C, (b) 800°C and morphology of IP deposited with a gas preheat temperature of (c) 400°C, (d) 800°C. In (c) and (d) arrows emphasize regions of jetting in IP splats.

### 3.2. Splat adhesion test

#### 3.2.1. Spherical powder

The splat adhesion strengths for SP are shown in figure 4 (a). There is no statistical difference in splat adhesion strength with an increase in gas preheat temperature as verified by a t-test. SP splats deposited under both spray conditions result in Ti remaining on the substrate along the periphery of the splat (figure 4 (b)) as previously observed when depositing Ti on polished Al<sub>2</sub>O<sub>3</sub> [12]. The post-test morphology of Ti remaining on the substrate is referred to as an adhesion ring.

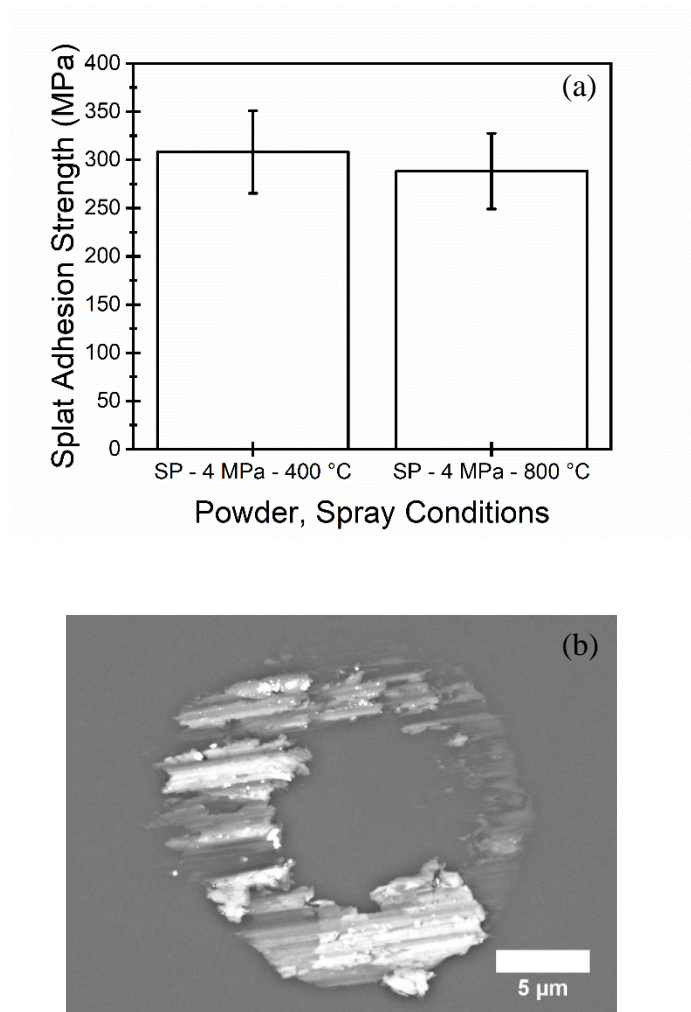


**Figure 4.** (a) Splat adhesion strength of single SP splats deposited at 400°C and 800°C. (b) Failed interface of an SP splat showing an ‘adhesion ring’.

Six frames recorded for a single SP splat, deposited at 400°C, during *in situ* splat adhesion testing are shown in figure 5. Observations of failure for SP splats deposited at 800°C (not shown here) are identical to those deposited at 400°C. For this splat, a center interface crack is visible in the first frame by a light contrast at the center of the splat. This center interface crack was repeatedly seen when observing through the substrate. However, due to the resolution of the LOM when recording through the sapphire substrate, the center crack is difficult to see. As the center begins to buckle under the tangential load of the tip, the center interface crack propagates and becomes more visible. Crack propagation continues through frames two to five, from the center outwards, until failure occurs instantly through the Ti (frame six) leaving a ring of material on the substrate. The ring remaining on the substrate is representative of well bonded material. Crack propagation occurs through the weakest part of the material. Therefore, the strength of the Ti is lower than the interface shear strength between the Ti and sapphire in the adhesion ring.

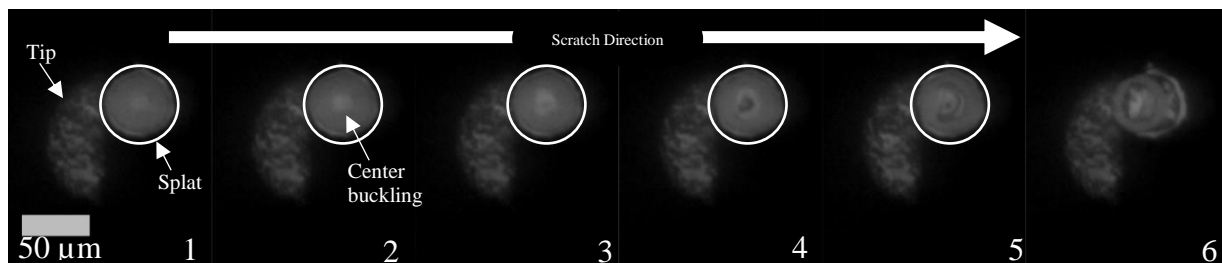


**Figure 5.** Six frames captured during *in situ* splat adhesion testing of a SP splat deposited at 400°C showing the typical failure dynamics in splat/substrate interfaces using SP where failure begins in the center with crack propagation outwards leaving a ring of Ti on the substrate.

Features identified in typical tangential force plots with respect to position (figure 6) match *in situ* observations. When the tip meets the splat, the tangential force increases. The increase is not perfectly linear as plastic deformation and crack propagations starts to occur. There is a sudden drop in the tangential force when splat failure occurs.

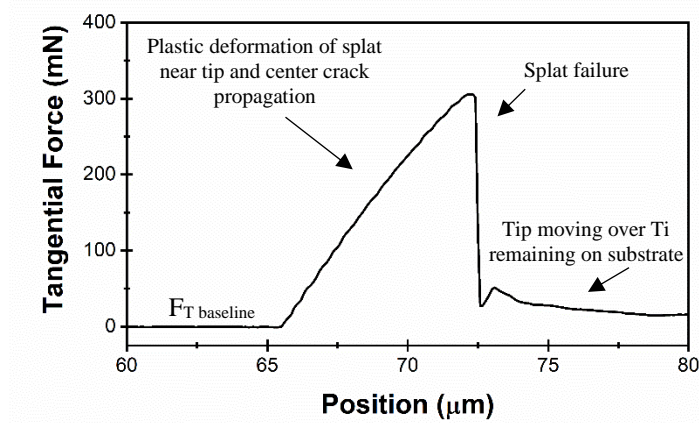


**Figure 6.** A representative tangential force with respect to position plot during sputter/substrate failure of SP deposited at 400°C.

### 3.2.2. Irregular powder

The increase in gas temperature has a more pronounced impact on IP (figure 7). At a gas pre-heat temperature of 400°C, IP have weak adhesion to the sapphire substrate. Increasing the gas pre-heat temperature to 800°C for IP significantly improves adhesion.

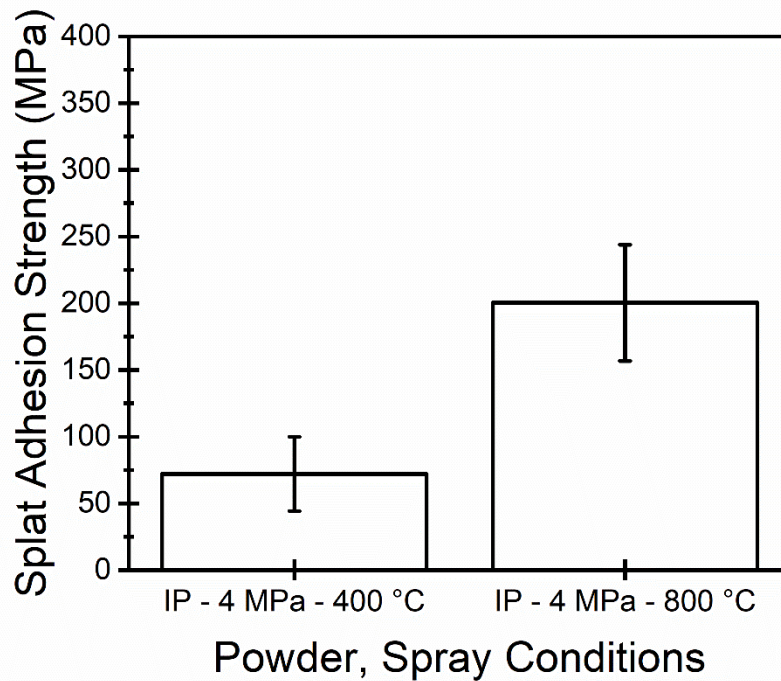


**Figure 7.** Splat adhesion strength of IP splats deposited at different gas pre-heat temperatures.

The footprint observed in post-test characterization (figure 8 (a, b)) is significantly different for both spray conditions. For IP splats deposited at 400°C, failed interfaces show localized adhesion rings (figure 8 (a)). These rings are a result of localized contact between the irregular shaped protrusions and the substrate which form a material jet through ASI similarly to SP. As previously shown (figure 3), IP show localized evidence of ASI which correlates with the localized adhesion rings found on the substrate following the splat adhesion test. In regions where jetting and ASI are formed, the Ti and sapphire form a bond. Due to the large amount of interface cracks propagating simultaneously, failure of the splat occurs rapidly (figure 9 (a)). The representative tangential force plot in figure 8 (c) show a drop shortly after contact with the splat. When testing IP splats, the shape of the peak may be slightly different from one splat to another given the irregular nature of the bond formed. However, general observations as previously mentioned remain valid. This rapid crack propagation is further confirmed by *in situ* observation of failure during splat adhesion testing for splats deposited at 400°C (figure 9 (a)). Cracks start to propagate in many locations through the interface (frame 2). These cracks continue to propagate until failure of the splat (frame 3 to 5).

For particles deposited at 800°C, only few splats experience interface failure even when increasing the normal force in the splat adhesion test. Failed interfaces include a large amount of Ti remaining on the substrate in the shape of the scratched splat (figure 8 (b)). There is some evidence of interface cracks as identified by arrows in figure 8 (b) but these are less prominent than for SP or IP deposited at 400°C and appear to minimally affect failure. Since failure does not occur in the interface, Ti is sheared near the interface as observed in *in situ* observation of failure (figure 9 (b)). Tangential force plots consistently show a peak with no drastic drop (figure 8 (d)). The particle fails before the tip has traveled over the entire splat. Given that failure occurs through the Ti, the tip continues to shear residual Ti on the surface. Therefore, the tangential force does not return to the baseline after failure. For splat adhesion energy calculations, the area under the curve is taken up to the initial peak drop as it is more representative of the splat failure.

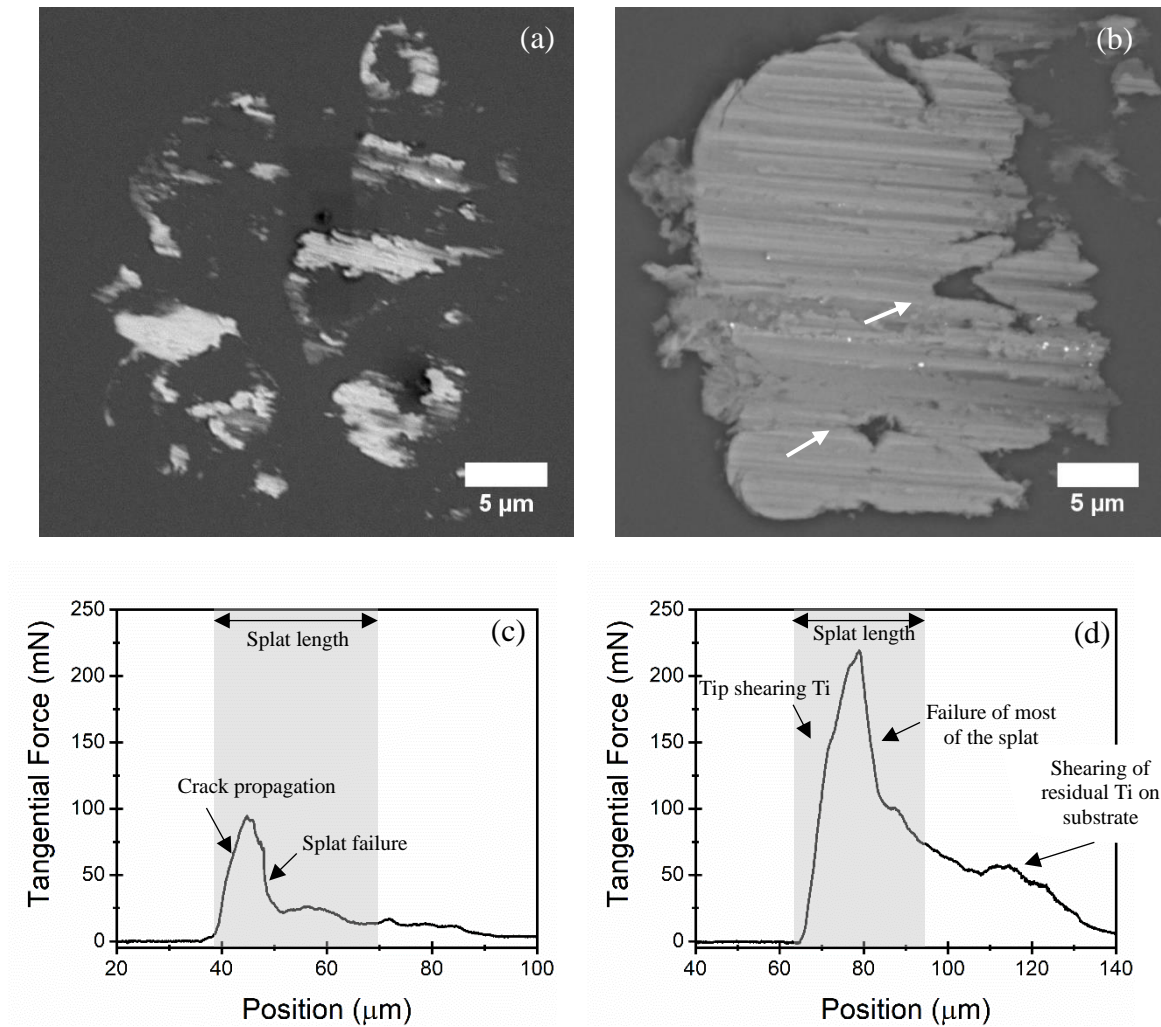


**Figure 8.** Failed interface and tangential force versus position plot for a IP splat deposited at (a, c) 400°C and (b, d) 800°C

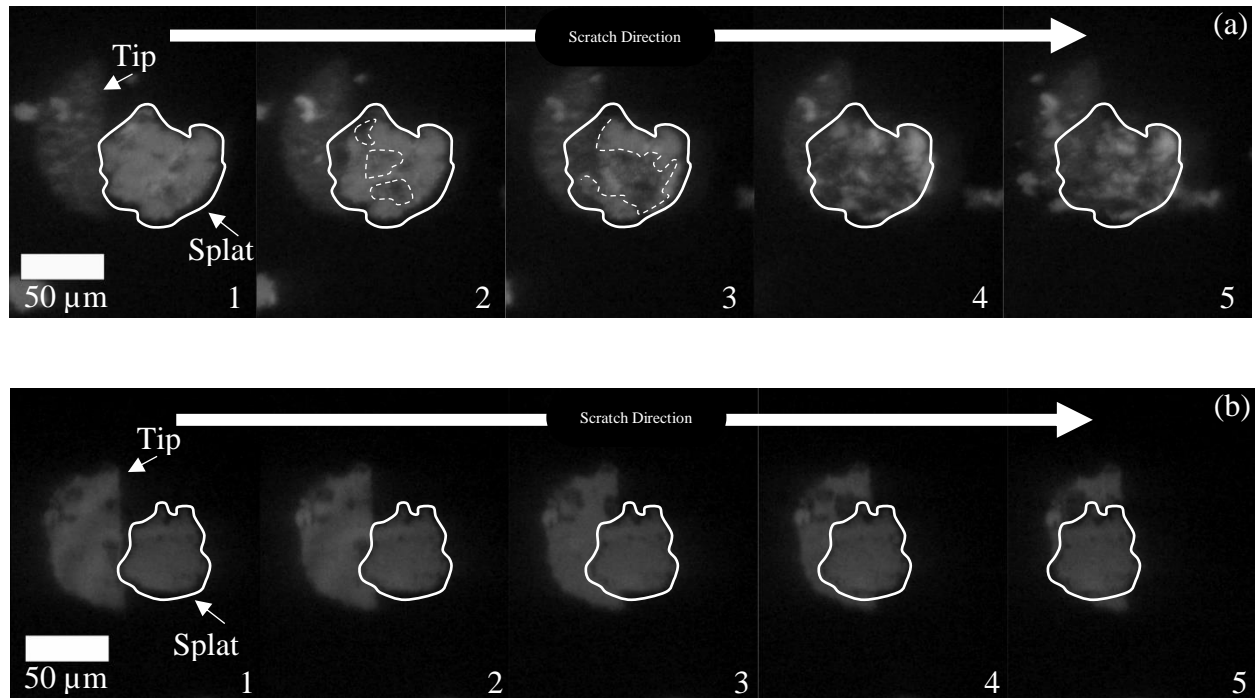


**Figure 9.** Five frames captured through the sapphire substrate during *in situ* splat adhesion testing for IP splats deposited at a gas preheat temperature of (a) 400°C and (b) 800°C showing the failure dynamics of these interfaces.

No crack propagation in the interface between the IP splats deposited at 800°C and the substrate is indicative of a continuous well bonded interface. Given the irregular shape of the powder, at higher velocities, more shear contact may occur in the Ti/sapphire interface resulting in less interface defects. Despite the continuous and well bonded interface between IP splats deposited at 800°C and the sapphire, splat adhesion strength is lower than SP splats deposited under the two spray conditions. However, the splat adhesion energy is higher for the IP splats deposited at 800°C than that of the SP splats under both spray conditions (figure 10). The higher splat adhesion energy is indicative of a more ductile failure occurring through the Ti. SP splats deposited at both spray conditions and IP splats deposited at 400°C experienced a more brittle failure due to interface crack propagation. Therefore, while IP deposited at 800°C has a lower splat adhesion strength, it has better cohesion to the substrate.

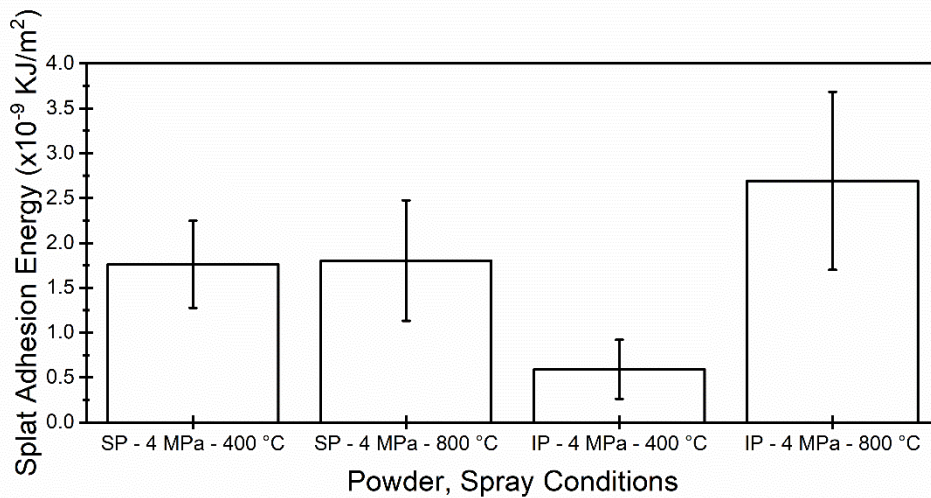


**Figure 10.** Splat adhesion energy for the SP and IP deposited at both spray conditions

Cross-sectional electron channelling contrast images (ECCI) are captured for the IP splats deposited under both spray conditions to better understand the splat adhesion test results. The IP splats deposited at 400°C (figure 11) show significantly less deformation than IP splats deposited at 800°C (figure 12). The IP splat deposited at 400°C have a combination of fine grains and coarser deformed grains at the interface (figure 11 (a, c)). The splat largely retains its initial microstructure but coarse grains near the interface show significantly more deformation. Near the interface, there is also no evidence of the large irregularly shaped pores typically found in the initial powder particles. The pores appear to collapse during impact. In the top portion of the splat, there is less deformation and more porosity.

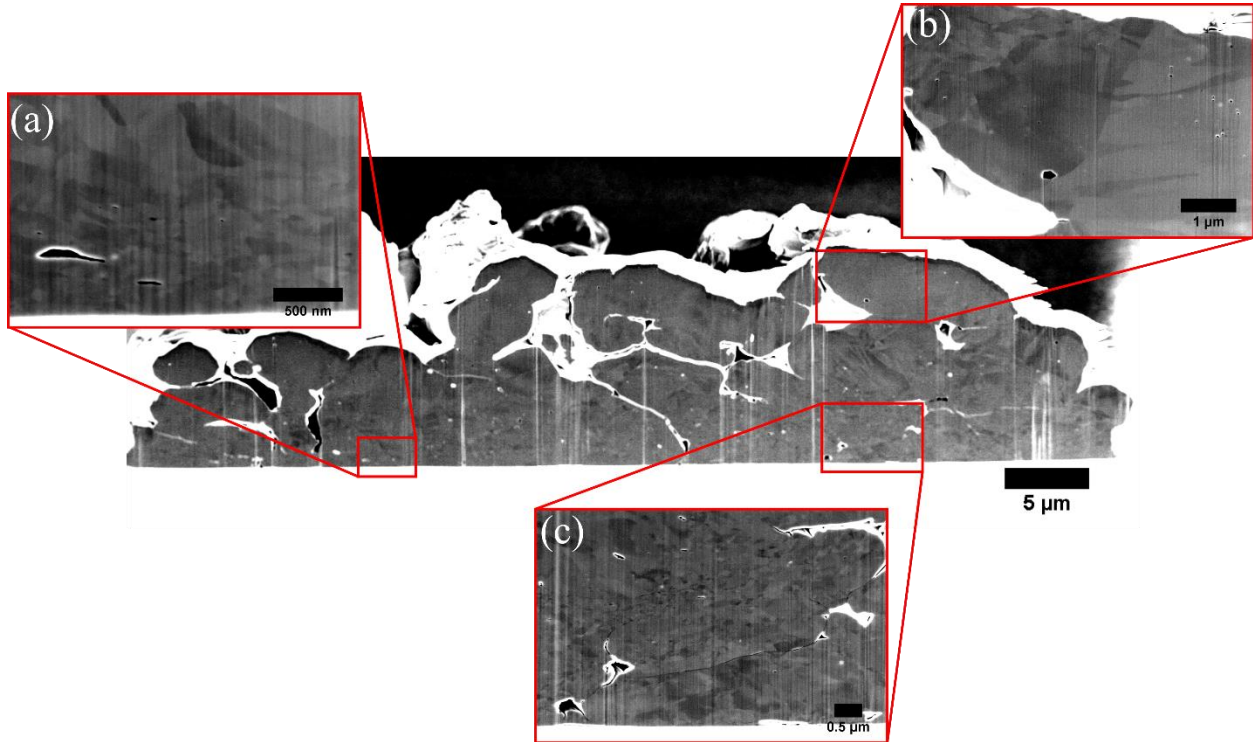


**Figure 11.** Microstructure of the IP Ti splat deposited at 400°C showing (a) fine grains in localized regions near the interface whereas (c) larger grains are also observed in the Ti along the interface. At the top of the splat, (b) large grains reflective of the initial powder microstructure are observed.

For IP deposited at 800°C, there are ultrafine grains along the entire interface with sapphire extending into the particle to a height of  $1 \pm 0.4 \mu\text{m}$ . Beyond the ultrafine grains, there is a region of fine grains followed by heavily deformed coarse grains. The splat appears completely deformed with minor evidence of initial powder microstructure at the top region. The amount of deformation in the coarse grains is not reflective of the initial powder. There is also significantly less porosity throughout the splat as compared to the splat deposited at 400°C. The protrusions conform to one another through the entire height of the splat but some fine interface pores between the protrusions are still present. At the interface there are some small pores as expected from post-test characterization results (figure 8 (b)).

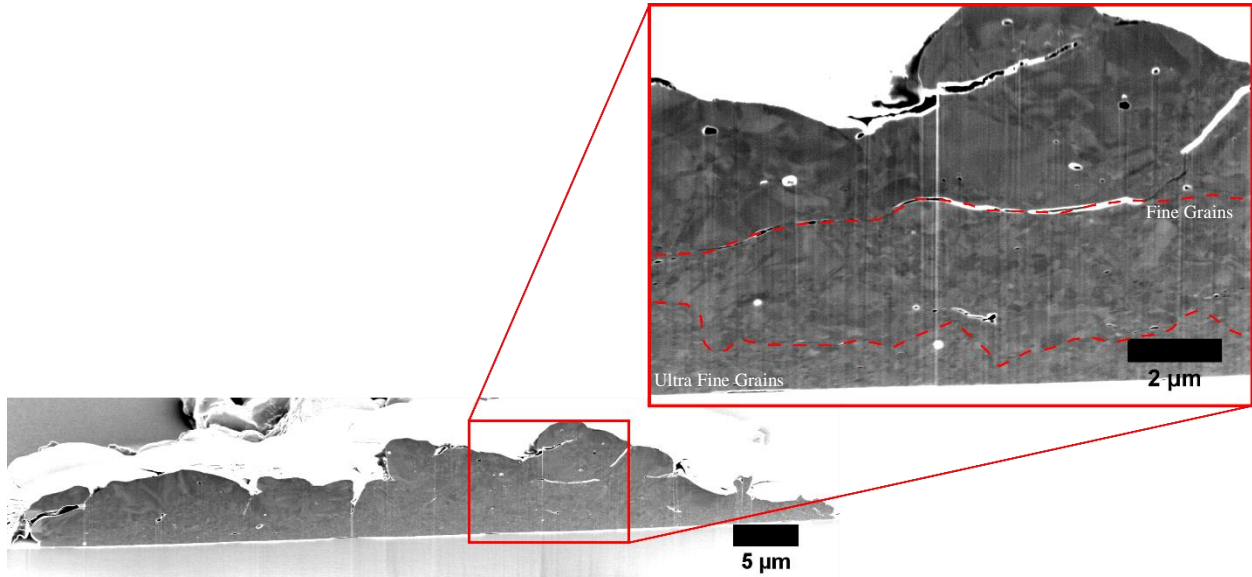


**Figure 12.** Microstructure of the IP Ti splat deposited at 800°C showing ultrafine grains throughout the entire interface that extends into the splat and leads to a region of fine grains. There is minor evidence of the initial microstructure in the top portion of the splat.

## 4. Discussion

### 4.1. Velocity

In this work, powder in-flight velocity was increased by increasing gas pre-heat temperature from 400°C to 800°C (Table 1). Previous work on Ti/Al<sub>2</sub>O<sub>3</sub> interfaces showed that temperature has a secondary influence on deformation and splat adhesion strength for the Ti/Al<sub>2</sub>O<sub>3</sub> interface while velocity plays a primary role [13]. Deformation and splat adhesion strength are less affected by gas preheat temperature as the contact time between the gas and the powder particles is short which limits heat transfer as previously investigated for Ti by a numerical model [13].

For the nozzle used, the maximum gas preheat temperature is 800°C. As observed previously [19, 20], for a given spray condition, IP achieves higher in-flight velocity than SP. Changes in velocity had very little effect on the splat adhesion strength of Ti/Al<sub>2</sub>O<sub>3</sub> interface using SP. While it is possible to achieve higher velocities with a different nozzle or by using helium as the working gas, many studies on cold spray have shown that splats from SP always have a small unbonded section near the center of the impact [14-17, 24]. Goldbaum, et al. [15] used helium to achieve higher

velocities for cp-Ti and Ti6Al4V splats onto Ti substrates. The effect of higher velocities with helium had minimal influence on the splat adhesion strength measured by the same techniques used here. For IP, increased velocity did result in an increase in splat adhesion strength. For the IP sprayed at the highest condition, deformation resulting in nearly full closure of all pores was observed. Higher spray conditions might lead to better adhesion, but previous studies by our group have shown that eventually fracture of the alumina occurs leading to a drop in splat adhesion strength [13].

#### **4.2. Impact induced deformation and bond formation**

Above a certain critical velocity, the impact of cold sprayed splats results in jetting and ASI in the periphery of the splat [16, 25]. Jetting and ASI induce microstructural changes in the deformed material [24, 26-29]. For SP, these microstructural changes have been well characterized in the literature and appear consistent for various material interfaces. The severe plastic deformation, occurring in the material jet, causes an ultrafine grain microstructure near the interface particularly in the periphery of the splat [16, 24, 27, 30]. ASI formation requires a certain contact angle to induce viscoplastic deformation as understood by experiments on explosive welding. The angled contact is prevented in the nearly parallel contact at the south pole of the splat [24]. Here, it is shown that adhesion for a spherical Ti powder particle deposited on sapphire occurs along the periphery of the splat where ultrafine grains are typically found similarly to metal/metal interfaces. These results are also comparable to those found when spraying Ti on polished polycrystalline Al<sub>2</sub>O<sub>3</sub> substrates [12] and zirconia [17]. Grain refinement and potential amorphization which can occur at the interface is associated with a reorientation of interface atoms which can form a heteroepitaxial bond in the metal/ceramic interface as previously described in the literature [3, 9, 31-33]. Therefore, the extent of deformation experienced by a single particle is significant to bond formation and is manifested by the amount of grain refinement observed in the splat/substrate interface.

The negligible effect of spray conditions on the splat adhesion strength of SP may be associated with the contact angle required for viscoplastic deformation. This would therefore be a geometric limitation to forming a more continuous bond. By use of geometry (figure13), the minimum angle required to form a bond between Ti and sapphire can be approximated. The point 'b', where the Ti begins to bond to the substrate, is assumed to be at the required contact angle for adhesion to

occur. The arc 'ab' is assumed to flatten as the particle impacts the substrate. As point 'b' comes in contact with the substrate, its angle with the substrate will be approximately ' $\theta$ '. The radius of the center pore is approximately equivalent to the length of the arc 'ab' and can be used to calculate the angle ' $\theta$ ' allowing for adhesion in each splat. Using this methodology for SP splats deposited at 400°C and SP splats deposited at 800 °C, the calculated angles are  $30 \pm 4^\circ$  and  $27 \pm 3^\circ$  respectively. Given the relatively consistent angle measured despite an increase in velocity, the geometric limitation is believed to be a significant factor affecting the adhesion of single spherical Ti splats. In metal/metal interfaces, the center pore reduces in size as velocity is increased [24]. Potentially, the deformation of the substrate or some surface roughness would render the conditions more favourable to minimizing the size of the center pore when depositing single SP splats of Ti. Here, for the atomically smooth sapphire substrate that shows no evidence of deformation, adhesion appears highly affected by contact angle.

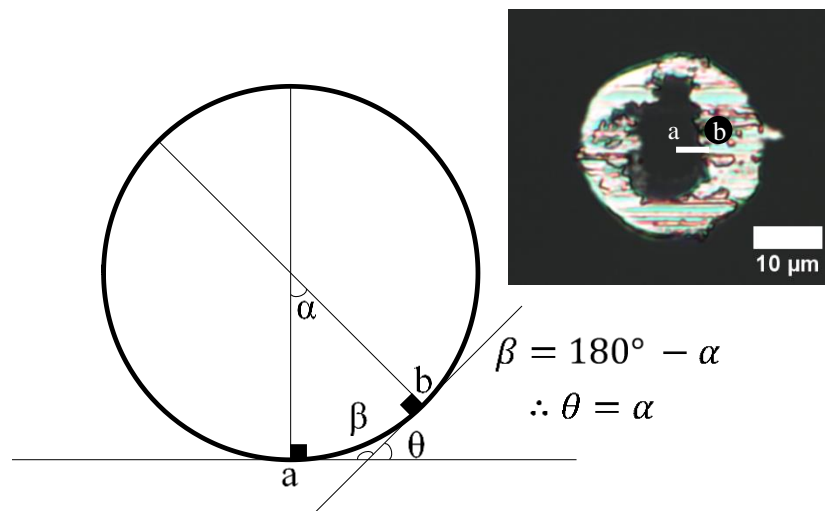


**Figure 13.** Contact angle between specified points on the circumference of the splat and the substrate.

When depositing a full coating, tamping from the impact of succeeding particles reduces porosity in the coatings/substrate interface that may be caused by such geometric limitations [34]. The specifically engineered coral-like morphology of the IP powder particles, used here, causes tamping within individual powder particles at high velocities rendering a continuous bond at the splat level. Geometric limitations in SP are therefore prevented by use of IP manufactured by the

Armstrong process. Individual IP particles can be considered as an agglomerated matrix of small powder particles of irregular shape. Protrusions near the interface are initially deformed. The collapse of the powder's initial internal porosity causes tamping of the first layer of protrusions in contact with the substrate. At high velocity, this continued compaction from tamping effects allows for a nearly continuous interface with the substrate.

The behaviour of the IP during impact, described above, is based on the observation of splat cross-sections and splat adhesion results. When deposited at low velocity, the IP splats show deformation near the interface but in the top portion of the splat there is a significant amount of porosity which is reflective of the initial powder's porosity (figure 11). The spray condition used is not adequate to cause complete deformation of the powder particle. Only protrusions near the interface are deformed and cause localized ASI at the multiple contact points. The localized ASI cause localized, irregularly shaped, adhesion rings in post-test characterization of failed interfaces (figure 8 (a)) allusive to the rings formed in SP splats. For IP splats deposited at a higher velocity, there is a complete collapse of internal porosity (figure 12). The reduced pore size is indicative of the higher strain experienced by the splat at impact. This collapse of internal porosity in the IP splats deposited at higher velocities causes tamping as previously discussed which allows for a complete deformation of the splat near the interface as identified by the ultrafine grains throughout the entire Ti/Sapphire interface.

### **4.3. Splat adhesion strength and fractography**

SP splats showed similar splat adhesion strength results at both spray conditions (figure 4 (a)). From *in situ* observation of fracture during the splat adhesion test, the center interface crack acts as a stress concentration site under the applied load of the semi-circular tip (figure 5). As the critical stress for crack propagation is reached, the crack begins to propagate along the interface where adhesion is comparatively weak. Farther away from the center where ASI lead to a strong bond, the crack continues to propagate through the Ti. Crack propagation occurs rapidly causing a nearly instant drop in the tangential force plot with respect to distance (figure 6). Similar observations are made for the IP splats deposited at low velocities. However, the reported splat adhesion strength results are significantly lower than those of SP splats (figure 7). The lower adhesion is related to the large amount of interface cracks which propagate simultaneously and ultimately lead to failure (figure 9 (a)). In both above-mentioned cases, the presence of interface cracks leads to a more

brittle failure of the splat when compared to the IP splats deposited at higher velocities. For these IP splats deposited at higher velocity, a more continuous interface is identified where interface failure under the loading condition is not achievable. While splat adhesion strength measurements show a lower value for IP splats deposited at higher velocities when compared to SP splats, these results cannot be directly compared. The splat adhesion strength result reported for the high velocity IP splats is the minimum splat adhesion strength limited by the shear strength of the Ti splat. Since failure occurs through the Ti before delamination at the interface, the interesting impact conditions induced by the coral-like morphology of IP splat are considered to render better cohesion between the splat and the substrate as compared to SP when deposited at high velocities. For IP splats deposited at higher velocity, the greater compaction and greater degree of recrystallization would naturally lead to better mechanical properties in a full coating. The mechanism of multiple tamping events due to the coral-like morphology seems to be especially effective for cold spray. These observations are consistent with previous research on full coatings made on metal substrates, where coating made with IP were found to have better mechanical properties than coatings made with SP [19, 20].

## 5. Conclusion

Ti splats of SP and IP were deposited onto sapphire under two spray conditions, differentiated by changes in temperature resulting in changes in velocity. *In situ* splat adhesion testing provided insight regarding the failure mechanism of each splat. The SP splats deposited under both spray conditions showed very similar splat adhesion strengths due to a similar center interface crack propagation. The center interface crack is likely present due to a geometric limitation preventing an angled contact at the south pole of the splat for the formation of ASI. Failed interfaces presented well bonded rings. It was, therefore, confirmed that material jetting and ASI is a prerequisite to adhesion. These rings were also observed in the failed interfaces of IP splats deposited at 400°C. The localized protrusions on IP deform at impact and result in localized jetting and ASI resulting in localized adhesion. These scattered ring formations in the interface caused a low splat adhesion strength due to simultaneous cracks propagating. Increasing the velocity by increasing the gas temperature to 800°C for IP allows for a higher splat adhesion strength due to tamping induced by the complete deformation of the splat. Deformation of the IP deposited at 800°C occurred through the entire interface while IP deposited at 400°C showed very little deformation as identified by

ECCI imaging. Failure of splats deposited at 800°C occurred through the Ti rather than at the interface. The failure of high velocity IP splats through the Ti allowed for a more ductile failure identified by a higher splat adhesion energy as compared to low velocity IP splats and SP splats. Therefore, the irregular shape of Armstrong Ti powder is conducive to the formation of a continuous interface with sapphire when deposited at sufficiently high velocities. In contrast, with the spray conditions used, SP powder could not form a continuous bond due to the characteristic center interface crack which led to a more brittle failure.

### **Acknowledgements**

The authors acknowledge the assistance of Dr. Maniya Aghasibeig, Dr. Phuong Vo and Jean-Francois Alarie at the National Research Council Canada for technical support with the cold spray equipment and the contributions of Rene Cooper from Cristal Metals for providing the irregular Ti powder. We also thank Weawkamol Leelapornpisit at the Facility for Electron Microscopy Research of McGill University for help with the FEI Helios NanoLab 660 and Stéphanie Bessette at the McGill Materials Services Electron Microscopy Labs for help with the SU8230. Also, this work was supported by the Natural Science and Engineering Research Council (NSERC) Strategic Grants Program.

## References

- [1] E. Irissou, J.G. Legoux, B. Arsenault, C. Moreau, Investigation of Al-Al<sub>2</sub>O<sub>3</sub> cold spray coating formation and properties, *J. Therm. Spray Technol.* **16** (2007) 661-668. <https://doi.org/10.1007/s11666-007-9086-8>.
- [2] T. Marrocco, D. McCartney, P. Shipway, A. Sturgeon, Production of titanium deposits by cold-gas dynamic spray: Numerical modeling and experimental characterization, *J. Therm. Spray Technol.* **15** (2006) 263-272. <https://doi.org/10.1361/105996306X108219>.
- [3] R. Drehmann, T. Grund, T. Lampke, B. Wielage, K. Manyoats, T. Schucknecht, D. Rafaja, Splat formation and adhesion mechanisms of cold gas-sprayed Al coatings on Al<sub>2</sub>O<sub>3</sub> substrates, *J. Therm. Spray Technol.* **23** (2014) 68-75. <https://doi.org/10.1007/s11666-013-9966-z>.
- [4] Q. Wang, K. Spencer, N. Birbilis, M.-X. Zhang, The influence of ceramic particles on bond strength of cold spray composite coatings on AZ91 alloy substrate, *Surf. Coat. Technol.* **205** (2010) 50-56. <https://doi.org/10.1016/j.surfcoat.2010.06.008>.
- [5] K. Spencer, D.M. Fabijanic, M.X. Zhang, The influence of Al<sub>2</sub>O<sub>3</sub> reinforcement on the properties of stainless steel cold spray coatings, *Surf. Coat. Technol.* **206** (2012) 3275-3282. <https://doi.org/10.1016/j.surfcoat.2012.01.031>.
- [6] R.R. Chromik, D. Goldbaum, J.M. Shockley, S. Yue, E. Irissou, J.G. Legoux, N.X. Randall, Modified ball bond shear test for determination of adhesion strength of cold spray splats, *Surf. Coat. Technol.* **205** (2010) 1409-1414. <https://doi.org/10.1016/j.surfcoat.2010.07.037>.
- [7] R.R. Chromik, Y. Zhang, Nanomechanical testing of third bodies, *Curr. Opin. Solid State Mater. Sci.* **22** (2018) 142-155. <https://doi.org/10.1016/j.cossms.2018.05.001>.
- [8] B. Wielage, T. Grund, C. Rupprecht, S. Kuemmel, New method for producing power electronic circuit boards by cold-gas spraying and investigation of adhesion mechanisms, *Surf. Coat. Technol.* **205** (2010) 1115-1118. <https://doi.org/10.1016/j.surfcoat.2010.06.020>.
- [9] C. Wüstefeld, D. Rafaja, M. Motylenko, C. Ullrich, R. Drehmann, T. Grund, T. Lampke, B. Wielage, Local heteroepitaxy as an adhesion mechanism in aluminium coatings cold gas sprayed on AlN substrates, *Acta Mater.* **128** (2017) 418-427. <https://doi.org/10.1016/j.actamat.2017.02.021>.
- [10] K.R. Ernst, J. Braeutigam, F. Gaertner, T. Klassen, Effect of substrate temperature on cold-gas-sprayed coatings on ceramic substrates, *J. Therm. Spray Technol.* **22** (2013) 422-432. <https://doi.org/10.1007/s11666-012-9871-x>.

- [11] K.-R. Donner, F. Gaertner, T. Klassen, Metallization of thin Al<sub>2</sub>O<sub>3</sub> layers in power electronics using cold gas spraying, *J. Therm. Spray Technol.* **20** (2011) 299-306. <https://doi.org/10.1007/s11666-010-9573-1>.
- [12] S.I. Imbriglio, N. Brodusch, M. Aghasibeig, R. Gauvin, R.R. Chromik, Influence of substrate characteristics on single Ti splat bonding to ceramic substrates by cold spray, *J. Therm. Spray Technol.* **27** (2018) 1011-1024. <https://doi.org/10.1007/s11666-018-0743-x>.
- [13] S.I. Imbriglio, M. Hassani-Gangaraj, D. Veysset, M. Aghasibeig, R. Gauvin, K.A. Nelson, C.A. Schuh, R.R. Chromik, Adhesion strength of titanium particles to alumina substrates: A combined cold spray and LIPIT study, *Surf. Coat. Technol.* **361** (2019) 403-412. <https://doi.org/10.1016/j.surfcoat.2019.01.071>.
- [14] M.V. Vidaller, A. List, F. Gaertner, T. Klassen, S. Dosta, J.M. Guilemany, Single impact bonding of cold sprayed Ti-6Al-4V powders on different substrates, *J. Therm. Spray Technol.* **24** (2015) 644-658. <https://doi.org/10.1007/s11666-014-0200-4>.
- [15] D. Goldbaum, J.M. Shockley, R.R. Chromik, A. Rezaeian, S. Yue, J.G. Legoux, E. Irissou, The effect of deposition conditions on adhesion strength of Ti and Ti6Al4V cold spray splats, *J. Therm. Spray Technol.* **21** (2012) 288-303. <https://doi.org/10.1007/s11666-011-9720-3>.
- [16] T. Schmidt, F. Gartner, H. Assadi, H. Kreye, Development of a generalized parameter window for cold spray deposition, *Acta Mater.* **54** (2006) 729-742. <https://doi.org/10.1016/j.actamat.2005.10.005>.
- [17] K. Kim, M. Watanabe, S. Kuroda, Bonding mechanisms of thermally softened metallic powder particles and substrates impacted at high velocity, *Surf. Coat. Technol.* **204** (2010) 2175-2180. <https://doi.org/10.1016/j.surfcoat.2009.12.001>.
- [18] D. Rafaja, T. Schucknecht, V. Klemm, A. Paul, H. Berek, Microstructural characterisation of titanium coatings deposited using cold gas spraying on Al<sub>2</sub>O<sub>3</sub> substrates, *Surf. Coat. Technol.* **203** (2009) 3206-3213. <https://doi.org/10.1016/j.surfcoat.2009.03.054>.
- [19] D. MacDonald, R. Fernández, F. Delloro, B. Jodoin, Cold spraying of armstrong process titanium powder for additive manufacturing, *J. Therm. Spray Technol.* **26** (2017) 598-609. <https://doi.org/10.1007/s11666-016-0489-2>.
- [20] V.N.V. Munagala, V. Akinyi, P. Vo, R.R. Chromik, Influence of powder morphology and microstructure on the cold spray and mechanical properties of Ti6Al4V coatings, *J. Therm. Spray Technol.* **27** (2018) 827-842. <https://doi.org/10.1007/s11666-018-0729-8>.

- [21] V.N.V. Munagala, S.I. Imbriglio, R.R. Chromik, The influence of powder properties on the adhesion strength and microstructural evolution of cold sprayed Ti6Al4V single splats, *Mater. Lett.* **244** (2019) 58-61. <https://doi.org/10.1016/j.matlet.2019.02.028>.
- [22] K. Araci, D. Mangabhai, K. Akhtar, 9 - Production of Titanium by the Armstrong Process®, in: M. Qian, F.H. Froes (Eds.) *Titanium powder metallurgy*, Butterworth-Heinemann, Boston, 2015, pp. 149-162.
- [23] J.I. Goldstein, D.E. Newbury, P. Echlin, D.C. Joy, C.E. Lyman, E. Lifshin, L. Sawyer, J.R. Michael, *Special Topics in Scanning Electron Microscopy*, in: *Scanning Electron Microscopy and X-Ray Microanalysis: Third Edition*, Springer US, Boston, MA, 2003, pp. 195-270.
- [24] H. Assadi, H. Kreye, F. Gärtner, T. Klassen, Cold spraying – a materials perspective, *Acta Mater.* **116** (2016) 382-407. <https://doi.org/10.1016/j.actamat.2016.06.034>.
- [25] T. Schmidt, H. Assadi, F. Gartner, H. Richter, T. Stoltenhoff, H. Kreye, T. Klassen, From particle acceleration to impact and bonding in cold spraying, *J. Therm. Spray Technol.* **18** (2009) 794-808. <https://doi.org/10.1007/s11666-009-9357-7>.
- [26] K. Kim, M. Watanabe, J. Kawakita, S. Kuroda, Grain refinement in a single titanium powder particle impacted at high velocity, *Scr. Mater.* **59** (2008) 768-771. <https://doi.org/10.1016/j.scriptamat.2008.06.020>.
- [27] C. Lee, J. Kim, Microstructure of kinetic spray coatings: A review, **24** (2015) 592-610. <https://doi.org/10.1007/s11666-015-0223-5>.
- [28] H. Assadi, F. Gärtner, T. Stoltenhoff, H. Kreye, Bonding mechanism in cold gas spraying, *Acta Mater.* **51** (2003) 4379-4394. [https://doi.org/10.1016/S1359-6454\(03\)00274-X](https://doi.org/10.1016/S1359-6454(03)00274-X).
- [29] M. Grujicic, C.L. Zhao, W.S. De Rosset, D. Helfritch, Adiabatic shear instability based mechanism for particles/substrate bonding in the cold-gas dynamic-spray process, *Mater. Des.* **25** (2004) 681-688. <https://doi.org/10.1016/j.matdes.2004.03.008>.
- [30] D. Goldbaum, R.R. Chromik, N. Brodusch, R. Gauvin, Microstructure and mechanical properties of Ti cold-spray splats determined by electron channeling contrast imaging and nanoindentation mapping, *Microsc. Microanal.* **21** (2015) 570-581. <https://doi.org/10.1017/S1431927615000240>.
- [31] K.H. Ko, J.O. Choi, H. Lee, The interfacial restructuring to amorphous: A new adhesion mechanism of cold-sprayed coatings, *Mater. Lett.* **175** (2016) 13-15. <https://doi.org/10.1016/j.matlet.2016.03.132>.

This is the accepted version of:

[S I Imbriglio et al 2019 Surf. Topogr.: Metrol. Prop. 7 045002 DOI: 10.1088/2051-672X/ab3efc](#)

[32] R. Drehmann, T. Grund, T. Lampke, B. Wielage, K. Manygoats, T. Schucknecht, D. Rafaja, Interface characterization and bonding mechanisms of cold gas-sprayed Al coatings on ceramic substrates, *J. Therm. Spray Technol.* **24** (2015) 92-99. <https://doi.org/10.1007/s11666-014-0189-8>.

[33] A. Viscusi, A. Astarita, R.D. Gatta, F. Rubino, A perspective review on the bonding mechanisms in cold gas dynamic spray, *Surf. Eng.* (2018) 1-29. <https://doi.org/10.1080/02670844.2018.1551768>.

[34] J. Villafuerte, *Modern Cold Spray : Materials, Process, and Applications*, Springer, Windsor, 2015.

## Table Caption

**Table 1** Velocity of IP and SP for each spray condition

## Figure Captions

**Figure 1.** The (a) powder size distribution and (b) morphology of the IP manufactured by the Armstrong process.

**Figure 2.** The microstructure of the IP manufactured by the Armstrong process. Arrows have been used to emphasize grains showing minor evidence of deformation.

**Figure 3.** Morphology of SP deposited with a gas preheat temperature of (a) 400°C, (b) 800°C and morphology of IP deposited with a gas preheat temperature of (c) 400°C, (d) 800°C. In (c) and (d) arrows emphasize regions of jetting in IP splats.

**Figure 4.** (a) Splat adhesion strength of single SP splats deposited at 400°C and 800°C. (b) Failed interface of an SP splat showing an ‘adhesion ring’.

**Figure 5.** Six frames captured during *in situ* splat adhesion testing of a SP splat deposited at 400°C showing the typical failure dynamics in splat/substrate interfaces using SP where failure begins in the center with crack propagation outwards leaving a ring of Ti on the substrate.

**Figure 6.** A representative tangential force with respect to position plot during splat/substrate failure of SP deposited at 400°C.

**Figure 7.** Splat adhesion strength of IP splats deposited at different gas pre-heat temperatures.

**Figure 8.** Failed interface and tangential force versus position plot for a IP splat deposited at (a, c) 400°C and (b, d) 800°C

**Figure 9.** Five frames captured through the sapphire substrate during *in situ* splat adhesion testing for IP splats deposited at a gas preheat temperature of (a) 400°C and (b) 800°C showing the failure dynamics of these interfaces.

**Figure 10.** Splat adhesion energy for the SP and IP deposited at both spray conditions

**Figure 11.** Microstructure of the IP Ti splat deposited at 400°C showing (a) fine grains in localized regions near the interface whereas (c) larger grains are also observed in the Ti along the interface. At the top of the splat, (b) large grains reflective of the initial powder microstructure are observed.

**Figure 12.** Microstructure of the IP Ti splat deposited at 800°C showing ultrafine grains throughout the entire interface that extends into the splat and leads to a region of fine grains. There is minor evidence of the initial microstructure in the top portion of the splat.

**Figure 13.** Contact angle between specified points on the circumference of the splat and the substrate.